Common-Loop MIMO Antenna Design With Decoupling Inductors Using Characteristic Mode Analysis

Longyue Qu, *Member, IEEE*

***Abstract*—This letter investigates the intrinsic operation principles of the decoupling inductors in multiple-input–multiple-output (MIMO) antenna design using the characteristic mode analysis, in the first of its kind. This work starts with the analysis of a conventional one-wavelength loop antenna and then investigates the MIMO antenna design methods in terminal scenarios. It is revealed that the decoupling inductors introduce a new characteristic mode within the antenna operation band, contributing to the current-mode-canceling effect and responsible for port-to-port isolation. A two-in-one common-loop MIMO antenna design with high-isolation characteristics is proposed for N77/N78/N79 applications. Both simulation and measurement were conducted to verify the feasibility of the proposed MIMO antennas.**

***Index Terms*—Characteristic mode analysis (CMA), decoupling inductor, high isolation, multiple-input–multiple-output (MIMO).**

I. Introduction

In WIRELESS communications, the multiple-input–multiple-output (MIMO) technology plays a critical role in increasing the channel capacity [1]. Nevertheless, decoupling and decorrelation have always been challenging work for MIMO antennas, especially when the antenna elements are closely allocated. Therefore, MIMO antennas have been extensively studied to obtain high integration, and miniaturization, especially for terminal devices.

In the literature, various decoupling techniques have been proposed, including neutralization lines, decoupling networks, parasitic elements, and diversity control [2], [3], [4], [5], [6], [7], [8], [9], [10], [11], [12], [13], [14], [15]. Among all, decoupling components (e.g., inductors, capacitors, or equivalent connection lines) are particularly of interest due to their advantages in compactness, tuneability, and integration [10], [11], [12], [13], [14], [15]. In [11], a new current mode was produced by using inductors, and this mode was exploited in the construction of MIMO antennas based on modal orthogonality. In [12], decoupling inductors and capacitors were introduced between monopole-type antennas to improve the isolation even though the antenna elements were closely arranged. The decoupling inductors and equivalent connecting lines were further studied in [13], where the analysis of the common mode and the differential mode was first presented. Recently, the mode cancellation method has been a popular method to explain the decoupling principle of MIMO antennas [14]. Still, a qualitative analysis of the decoupling components is necessary such that the underlying operation mechanism could be better understood and more innovative solutions could be possibly explored.

Herein, characteristic mode analysis (CMA) has been a critical tool that provides researchers with a straightforward and intuitive insight into MIMO antenna designs. For example, CMA of the ground plane have been analyzed to design multi-polarized antenna elements [16], [17], [18]. Furthermore, CMA could be utilized to investigate the user effects of multiple antennas [19], [20]. Besides, CMA also provides an important insight into single-radiator multiport patch antennas [21], [22]. To the best of the author's knowledge, the CMA of the decoupling-component-based MIMO antennas has yet to be reported in the literature.

Therefore, this letter presents a qualitative analysis of the decoupling inductors using CMA, and interesting discoveries have been observed by resolving the modal significance (MS). Besides, a wideband common-loop MIMO antenna design based on decoupling inductors is proposed for 5G terminal devices.

II. CMA of One-Wavelength Loop With Decoupling Inductors

A. Theory of Characteristic Mode

The theory of characteristic mode reveals that the current over the surface of an arbitrary conducting body can be decomposed into a linear combination of modal functions [23]. Accordingly, the modal solutions can be written as

$$\boldsymbol{J} = \sum_n \frac{\iiint (\boldsymbol{J}_n \cdot \boldsymbol{E}^i) d\tau}{1 + j\lambda_n} \boldsymbol{J}_n. \tag{1}$$

$\boldsymbol{J}_n$ is the characteristic current of the nth mode and $\boldsymbol{E}^i$ represents the external excitation. λ_n is the eigenvalue, and it is zero if $\omega = \omega_n$, where ω_n is the resonant frequency of the nth mode.

In practice, the term called MS is usually preferred to represent the modal solution, which is defined as

$$\mathrm{MS}_n = \left| \frac{1}{1 + j\lambda_n} \right|. \tag{2}$$

It represents the normalized amplitude of the current modes, and this normalized amplitude depends only on the shape and size of the conducting body and does not account for excitation. Now, the resonance of each mode can be identified by a maximum value of 1 in the MS curves. The nearest the curve is to the maximum value, the most effectively the related mode contributes to radiation.

Manuscript received 11 July 2023; accepted 5 September 2023. Date of publication 7 September 2023; date of current version 1 December 2023.

The author is with the School of Electronics and Information Engineering and Guangdong Provincial Key Laboratory of Aerospace Communication and Networking Technology, Harbin Institute of Technology (Shenzhen), Shenzhen 518055, China (e-mail: qulongyue@hit.edu.cn).

Digital Object Identifier 10.1109/LAWP.2023.3312690

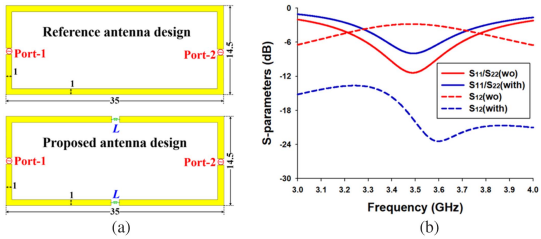

Fig. 1. Common-loop MIMO antennas. (a) Antenna configurations with and without decoupling inductors. (b) Simulated *S*-parameters.

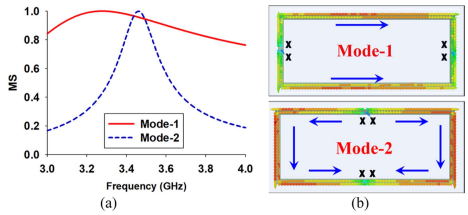

Fig. 2. CMA of the loop without the decoupling inductors. (a) MS curves. (b) Characteristic currents.

B. Decoupled One-Wavelength Loop

The loop antenna with a perimeter of one wavelength has been widely used because of its freedom in structural implementation and impedance adjustment [24]. A copolarized MIMO antenna design based on a rectangular one-wavelength loop is investigated here. As depicted in Fig. 1(a), a two-port common-loop antenna is designed, and two voltage ports are symmetrically loaded at the right-hand side and left-hand side of the loop for radiation. In the proposed antenna design, two decoupling inductors L are introduced at the center of the loop to improve the port-to-port isolation. The overall dimension of the loop is 14.5×35 mm^2, and the optimized value of the inductors (L) is 60 nH. It is noted that other shapes of the loop, such as a square loop or circular loop, could also be used for analysis.

The scattering parameters (*S*-parameters) in the simulation are plotted in Fig. 1(b). The port-to-port isolation (S_{12}) is significantly improved from 2.8 dB to higher than 20 dB. Accordingly, a common-loop MIMO antenna with copolarization and high-isolation properties is accomplished by merely using inductors.

C. CMA and Discussion

In the absence of the decoupling inductors, there are two characteristic modes near the resonance of 3.5 GHz, denoted as Mode-1 and Mode-2, as can be observed in Fig. 2(a). Their characteristic currents are plotted in Fig. 2(b), and it is known that Mode-1 and Mode-2 are the fundamental and quasidegenerate characteristic modes of the one-wavelength loop.

In the presence of the decoupling inductors, as shown in Fig. 3(a), Mode-1 is tuned out of the operation band because the loaded inductors are located at the current maximums of Mode-1. On the contrary, Mode-2 is barely affected because the inductors are located at the current null positions of Mode-2. Since Mode-2 is almost unchanged, we use a consistent name for Mode-2 ignoring the presence of the decoupling inductors. Interestingly, a new characteristic mode occurs, denoted as Mode-3. Mode-3 has an antiphase current flow when compared with that of Mode-2, along half part of the loop. Accordingly, the emergence of Mode-3 could be the key to the proposed decoupling technique.

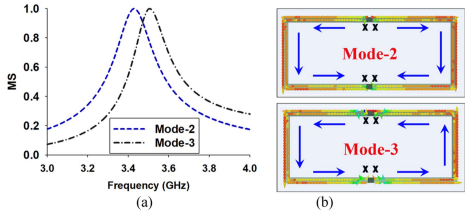

Fig. 3. CMA of the loop with the decoupling inductors. (a) MS curves. (b) Characteristic currents of the loop.

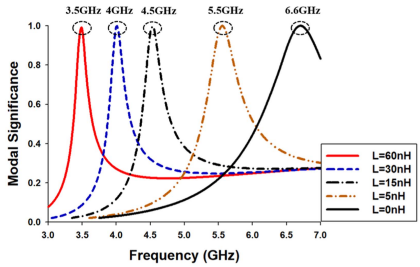

Fig. 4. MS variation of Mode-3 when the decoupling inductors are varied.

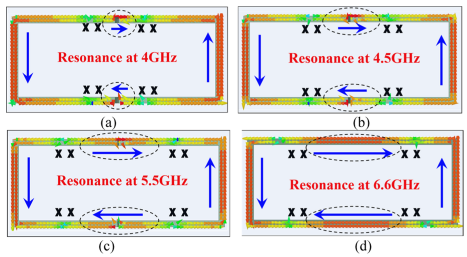

Fig. 5. Iteration of characteristic currents of Mode-3. (a) Inductor value of 30 nH. (b) Inductor value of 15 nH. (c) Inductor value of 5 nH. (d) Inductor value of 0 nH (without inductors).

Next, the derivation of Mode-3 is investigated by sweeping the inductor value and observing the MS variation.

It is observed from the curves in Fig. 4 that Mode-3 shifts to a higher frequency when the inductor value gradually decreases from 60 to 0 nH. Specifically, Mode-3 is operating at 4 GHz when $L = 30$ nH, 4.5 GHz when $L = 15$ nH, 5.5 GHz when $L = 5$ nH, and 6.6 GHz when the inductors are not loaded ($L = 0$ nH). Their characteristic currents are plotted in Fig. 5. By observing the progressive variation of the characteristic currents, it is concluded that Mode-3 is originally a high-order characteristic mode of the loop, whose resonance has an electrical length of two wavelengths with four current nulls. The inductors act as condensed conductor lines and carry all the current flows in the middle transverse section of the loop. In this way, the inductors lower the resonance of Mode-3 from 6.6 to 3.5 GHz without increasing the overall dimension of the loop. Therefore, the decoupling inductors are installed at the current null positions of Mode-2 and the current maximum positions of Mode-3 so that Mode-3 can be selectively controlled without affecting Mode-2.

D. Simulation Results and Discussion

To give intuitive insight into the role of Mode-3 in antenna decoupling, the surface current distributions of the MIMO antennas with and without the decoupling inductors are investigated (see Fig. 6).

In Fig. 6(a), Port 1 is excited in the absence of the decoupling inductors. In this case, the voltage source (Port 1) is strongly

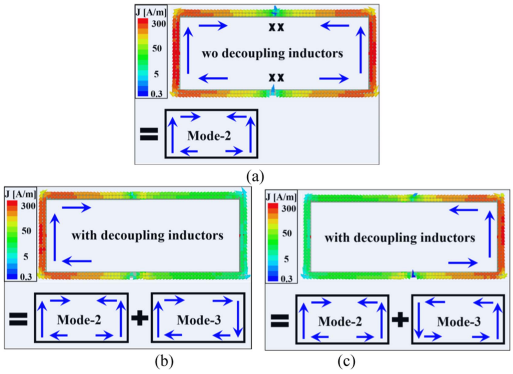

Fig. 6. Simulated current distributions. (a) Port 1 is excited without decoupling inductors. (b) Port 1 is excited with decoupling inductors. (c) Port 2 is excited with decoupling inductors.

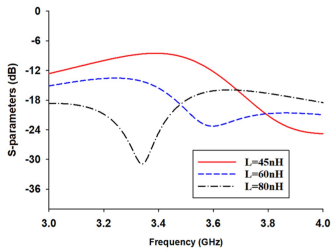

Fig. 7. Isolation variation when the decoupling inductors are varied.

coupled with Mode-2 only, so that a one-wavelength loop-type current distribution is produced, having current maxima on the right-hand and left-hand sides of the loop. Therefore, a strong mutual coupling is induced from one port to another because of the CM (Mode-2). Similar results will be generated when Port 2 is excited, which is omitted here for simplicity. In Fig. 6(b), Port 1 is excited in the presence of the decoupling inductors. In this case, the voltage source (Port 1) is coupled with Mode-2 and Mode-3 simultaneously, then the total current distribution produced by Port 1 is a summation of Mode-2 and Mode-3. Since Mode-2 and Mode-3 have an antiphase current flow along half part of the loop, as presented in Fig. 3(b), the superposition of Mode-2 and antiphase Mode-3 is enhanced on the left half side and is canceled on the right half side of the loop. Consequently, the produced current distribution by Port 1 is concentrated only on the left half side of the loop, indicating that the left half side and the right half side of the loop are isolated, i.e., Port 1 is isolated from Port 2. Similarly, in Fig. 6(c), Port 2 is excited and the produced current distribution is concentrated only on the right half side of the loop.

Further investigation on the decoupling inductors is presented in Fig. 7. It is seen that the isolation improves when L is increased from 45 to 60 nH because Mode-3 is lowered into the antenna operating frequency band. A further increase of L from 60 to 80 nH, on the contrary, decreases the isolation because Mode-3 is moving out-of-band. Accordingly, the decoupling property is well controlled by shifting Mode-3, which can be simply done by adjusting the inductor value.

Therefore, CMA reveals the underlying operation mechanism of the decoupling inductors in loop MIMO antennas. Some important conclusions are summarized as follows.

1) The high-order mode (Mode-3) is lowered into the antenna's operating frequency band by loading decoupling inductors without affecting the original antenna mode (Mode-2).

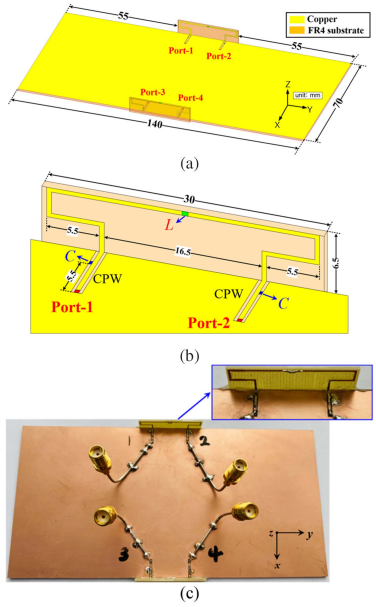

Fig. 8. Decoupled common-loop MIMO antenna. (a) Overall configurations. (b) Zoomed view of the modular board. (c) Fabricated prototype.

2) The lowered Mode-3 and Mode-2 have an antiphase current flow along half part of the loop, and the creation of antiphase Mode-3 is a particular feature of the proposed decoupling technique.
3) Coexist and simultaneous excitation of the original antenna mode (Mode-2) and the antiphase high-order mode (Mode-3) introduce a mode-current- cancelation effect on the half side of the loop.

This exploration is also consistent with the reported MCM in [14] and explains the operation mechanism of previously reported decoupling inductors or equivalent connecting lines [11], [12], [13], [14], [15].

III. MIMO Antenna Design for Terminal Applications

Based on the aforementioned investigation, this section presents the decoupling-inductor-based MIMO antenna design method in terminal scenarios. First, the common-loop MIMO antennas are installed onto the ground plane, and according to the image theory, the perimeter of the loop on the ground plane would be half of an independent loop [24]. Afterward, the loop structure is meandered for antenna miniaturization. Finally, the impedance matching and the inductor value are optimized. Detailed information is described as follows.

A. Decoupled Common-Loop MIMO Antenna

A two-in-one common-loop MIMO antenna module with a decoupling inductor is presented, and the configurations are depicted in Fig. 8(a). The ground plane has a dimension of 70 $\times$ 140 mm^2 and is fabricated on a 1 mm-thick FR4 substrate ($\varepsilon_r = 4.4$, $\tan\delta = 0.02$). The loop MIMO antennas are etched on a 6.5 $\times$ 30 $\times$ 1 mm^3 modular board, vertically implemented at the edge side of the ground plane. The loop has a meandered structure with symmetry whose electrical length of the perimeter is around half wavelength at 3.5 GHz. Each end of the loop is connected to one voltage port through CPW lines, and a shunt capacitor C (0.4 pF) is utilized for impedance matching. A decoupling inductor L (45 nH) is loaded at the center of the

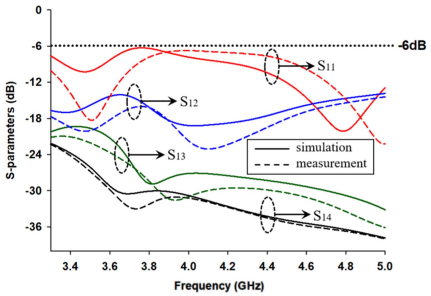

Fig. 9. Simulated and measured *S*-parameters.

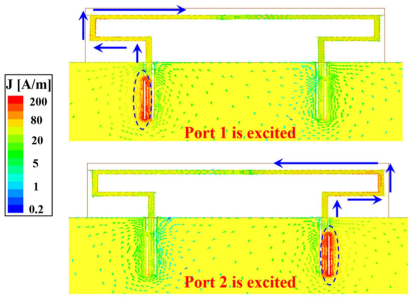

Fig. 10. Current distributions when ports 1 and 2 are excited, respectively.

upper trace of the loop for isolation improvement. Meanwhile, the width of all the conductor lines is 0.5 mm. It is noted that the antenna number could be possibly scaled up by deploying such antenna modules; in this case, two modules are implemented at the middle center of the ground plane for simplicity.

B. Simulated and Measured Results

Fabrication was conducted and its prototype is pictured in Fig. 8(c). The simulated and measured *S*-parameters are shown in Fig. 9. As can be observed, the S_{11}/S_{22} curves can fully cover the N77/N78/N79 frequency bands (more than 1700 MHz), and the mutual coupling between any two ports is lower than -15 dB in measurement. It is noted that the mutual coupling is as high as -5 dB when the inductors are removed (open circuit) or replaced by the conductor line (short circuit). The measured results are consistent with the simulated ones only with a minor discrepancy, which may be attributed to the fabrication error, cable effect, and extra loss from inductors. Note that Murata LQP series inductors are used in fabrication [25], whereas an ideal lumped inductor is modeled in the simulation. In practical scenarios, multiple series and parallel inductors could be an option for antenna tuning and optimization. It is important to notice that the core logic behind the decoupling inductors is control of the high-order mode resonance regardless of the inductor properties, e.g., the quality factors.

The simulated surface current distributions at 4 GHz are plotted in Fig. 10. The produced currents of Port 1 and Port 2 accumulate mostly on the left half side and right half side of the loop, respectively. Meanwhile, few currents are induced from one port to another, verifying their high-isolation property. As a result, each port is working as a quarter-wavelength monopole-type radiator. These current distributions are consistent with those in Fig. 6. Meanwhile, the inductance and capacitance in the feeding structure contribute to an additional feeding resonance, which is an important factor for the wideband characteristic.

In addition, Fig. 11 displays the produced far-field radiation patterns at 3.8 GHz in the *xz*-, *yz*-, and *xy*-planes. The proposed

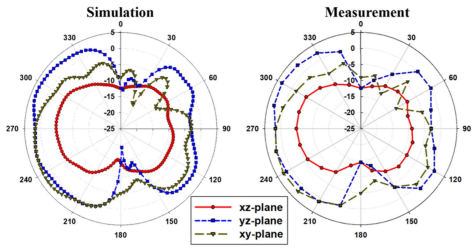

Fig. 11. Simulated and measured radiation patterns of Port 1 (symmetrical radiation pattern is observed in Port 2).

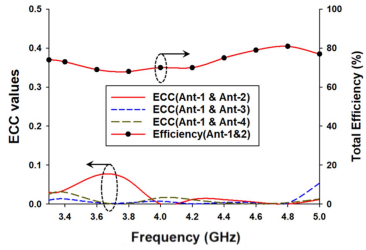

Fig. 12. Measured ECC values and total efficiencies of the fabricated antennas.

TABLE I
COMPARISON WITH THE STATE OF THE ART IN THE LITERATURE

Ref.	Decoupling method	Operation band	Isolation	Complexity
[9]	Polarization orthogonality	Dual-band	>15 dB; >12 dB	Complex
[10]	Orthogonal modes	Single-band	>18 dB	Medium
[11]	Orthogonal modes	Narrowband	>16 dB	Easy
[12]	Decoupling components	Narrowband	>11.6 dB	Easy
[13]	Connecting line	Wideband	>10.8 dB	Medium
This work	Decoupling inductor	Wideband	>15 dB	Easy

two-in-one MIMO antenna produces approximately complementary radiation patterns with maximum gains directed against each other, which is an attractive feature for signal reception. Correlation is an important factor to evaluate the diversity performance of MIMO antennas, which can be calculated from the vector properties (amplitude, phase, and polarization) of the far-field radiation patterns [26]. The calculated envelope correlation coefficient (ECC) ρ_e is plotted in Fig. 12, where the values are all below 0.1, which is much lower than the acceptable criterion ($\rho_e < 0.5$). In addition, the measured total efficiencies are also shown, and all antennas produced high radiation efficiencies of over 68% within the operation band.

Finally, a comparison with the state of the art in the literature is listed in Table I to further verify the novelty of the proposed technique. It can be verified that the proposed decoupling technique has advantages in wideband, high isolation, integration, and easy fabrication.

IV. CONCLUSION

CMA of the MIMO loop antenna with decoupling inductors reveals that the high-order characteristic mode is manipulated so that a new characteristic mode is generated in the antenna operation band. The current distinction between the new mode and the original mode determines the fact that the induced current from one port to another can be canceled, contributing to the decoupling effect. A two-in-one MIMO antenna with an impedance bandwidth of over 1700 MHz and high isolation above 15 dB is then presented for 5G applications. Meanwhile, the measured total efficiencies are higher than 68%, and the correlation between each two antennas is lower than 0.1.

REFERENCES

[1] A. Al-Wahhamy, H. Al-Rizzo, and N. E. Buris, "Efficient evaluation of massive MIMO channel capacity," *IEEE Syst. J.*, vol. 14, no. 1, pp. 614–620, Mar. 2020.

[2] K.-L. Wong, B.-W. Lin, and S.-E. Lin, "High-isolation conjoined loop multi-input multi-output antennas for the fifth-generation tablet device," *Microw. Opt. Technol. Lett.*, vol. 61, no. 1. pp. 111–119, Jan. 2019.

[3] Z. Xu and C. Deng, "High-isolated MIMO antenna design based on pattern diversity for 5G mobile terminals," *IEEE Antennas Wireless Propag. Lett.*, vol. 19, no. 3, pp. 467–471, Mar. 2020.

[4] Y. Q. Hei, J. G. He, and W. T. Li, "Wideband decoupled 8-element MIMO antenna for 5G mobile terminal applications," *IEEE Antennas Wireless Propag. Lett.*, vol. 20, no. 8, pp. 1448–1452, Aug. 2021.

[5] H. Xu, S. S. Gao, H. Zhou, H. Wang, and Y. Cheng, "A highly integrated MIMO antenna unit: Differential/common mode design," *IEEE Trans. Antennas Propag.*, vol. 67, no. 11, pp. 6724–6734, Nov. 2019.

[6] C.-Y.-D. Sim, H.-Y. Liu, and C.-J. Huang, "Wideband MIMO antenna array design for future mobile devices operating in the 5G NR frequency bands n77/n78/n79 and LTE Band 46," *IEEE Antennas Wireless Propag. Lett.*, vol. 19, no. 1, pp. 74–78, Jan. 2020.

[7] H. Piao, Y. Jin, and L. Qu, "A compact and straightforward self-decoupled MIMO antenna system for 5G applications," *IEEE Access*, vol. 8, pp. 129236–129245, 2020.

[8] X.-T. Yuan, Z. Chen, T. Gu, and T. Yuan, "A wideband PIFA-pair-based MIMO antenna for 5G smartphones," *IEEE Antennas Wireless Propag. Lett.*, vol. 20, no. 3, pp. 371–375, Mar. 2021.

[9] W. Hu et al., "Dual-band antenna pair with high isolation using multiple orthogonal modes for 5G smartphones," *IEEE Trans. Antennas Propag.*, vol. 71, no. 2, pp. 1949–1954, Feb. 2023.

[10] L. Qu and H. Piao, "A dual-port single-dipole MIMO antenna pair based on selective modal excitation for 5G metal-rimmed terminals," *IEEE Access*, vol. 10, pp. 100208–100214, 2022.

[11] A. Ren, Y. Liu, and C.-Y. Sim, "A compact building block with two shared-aperture antennas for eight-antenna MIMO array in metal-rimmed smartphone," *IEEE Trans. Antennas Propag.*, vol. 67, no. 10, pp. 6430–6438, Oct. 2019.

[12] C. Deng, D. Liu, and X. Lv, "Tightly arranged four-element MIMO antennas for 5G mobile terminals," *IEEE Trans. Antennas Propag.*, vol. 67, no. 10, pp. 6353–6361, Oct. 2019.

[13] L. Sun, Y. Li, and Z. Zhang, "Wideband decoupling of integrated slot antenna pairs for 5G smartphones," *IEEE Trans. Antennas Propag.*, vol. 69, no. 4, pp. 2386–2391, Apr. 2021.

[14] L. Sun, Y. Li, and Z. Zhang, "Decoupling between extremely closely spaced patch antennas by mode cancellation method," *IEEE Trans. Antennas Propag.*, vol. 69, no. 6, pp. 3074–3083, Jun. 2021.

[15] S.-C. Chen, C.-W. Chiang, and C.-I. G. Hsu, "Compact four-element MIMO antenna system for 5G laptops," *IEEE Access*, vol. 7, pp. 186056–186064, 2019.

[16] L. Qu, J. Jeon, D. Park, and H. Kim, "Antenna design based on quasi-degenerate characteristic modes of unbroken metal rim," *Microw., Antennas Propag.*, vol. 11, no. 15, pp. 2168–2173, Dec. 2017.

[17] Y. Liu, A. Ren, H. Liu, H. Wang, and C.-Y. Sim, "Eight-port MIMO array using characteristic mode theory for 5G smartphone applications," *IEEE Access*, vol. 7, pp. 45679–45692, 2019.

[18] C. Deng, Z. Xu, A. Ren, and S. V. Hum, "TCM-based bezel antenna design with small ground clearance for mobile terminals," *IEEE Trans. Antennas Propag.*, vol. 67, no. 2, pp. 745–754, Feb. 2019.

[19] H. H. Zhang, X. Z. Liu, G. S. Cheng, Y. Liu, G. M. Shi, and K. Li, "Low-SAR four-antenna MIMO array for 5G mobile phones based on the theory of characteristic modes of composite PEC-lossy dielectric structures," *IEEE Trans. Antennas Propag.*, vol. 70, no. 3, pp. 1623–1631, Mar. 2022.

[20] R. Luomaniemi, P. Y. Oijala, A. Lehtovuori, and V. Viikari, "Designing hand-immune handset antennas with adaptive excitation and characteristic modes," *IEEE Trans. Antennas Propag.*, vol. 69, no. 7, pp. 3829–3839, Jul. 2021.

[21] J.-F. Lin, H. Deng, and L. Zhu, "Design of low-profile compact MIMO antenna on a single radiating patch using simple and systematic characteristic modes method," *IEEE Trans. Antennas Propag.*, vol. 70, no. 3, pp. 1612–1622, Mar. 2022.

[22] L. Y. Nie, B. K. Lau, H. Aliakbari, S. Xiang, B. Wang, and X. Q. Lin, "A low-profile wideband dual-resonance tri-port MIMO antenna," *IEEE Trans. Antennas Propag.*, vol. 70, no. 6, pp. 4866–4871, Jun. 2022.

[23] R. F. Harrington and J. R. Mautz, "Theory of characteristic modes for conducting bodies," *IEEE Trans. Antennas Propag.*, vol. 19, no. 5, pp. 622–628, Sep. 1971.

[24] C. A. Balanis, *Antenna Theory: Analysis and Design*, 4th ed., Hoboken, NJ, USA: Wiley, 2016.

[25] Murata Manufacturing Co., Ltd. Selection guide for RF inductor. [Online]. Available: https://www.murata.com/en-us/products/inductor/chip/overview/lineup/rf1#lineup-area

[26] R. G. Vaughan, "Polarization diversity in mobile communications," *IEEE Trans. Veh. Technol.*, vol. 39, no. 3, pp. 177–186, Aug. 1990.